JOURNAL OF SOLID STATE CHEMISTRY 137, 62–70 (1998)
ARTICLE NO. SC977686

Synthesis, Structure, and Magnetic Properties of the New Ternary Nitride $BaHfN_2$ and of the $BaHf_{1-x}Zr_xN_2$ Solid Solution

D. H. Gregory,*,[1] M. G. Barker,* P. P. Edwards,† M. Slaski,‡ and D. J. Siddons*

*Department of Chemistry, The University of Nottingham, Nottingham NG7 2RD, United Kingdom;
†School of Chemistry, The University of Birmingham, Edgbaston, Birmingham B15 2TT, United Kingdom; and
‡School of Physics and Space Science, The University of Birmingham, Edgbaston, Birmingham B15 2TT, United Kingdom

Received July 23, 1997; in revised form October 20, 1997; accepted October 30, 1997

The new ternary nitrides $BaHf_{1-x}Zr_xN_2$ ($0 \leq x \leq 1$) have been synthesized by the solid state reaction of the binary nitrides Ba_3N_2, HfN, and ZrN and characterized by powder X-ray diffraction. The crystal structure of the end member, $BaHfN_2$, has been refined from powder data. The nitridohafnate crystallizes in the tetragonal space group *P4/nmm* ($a = 4.1279(1)$ Å, $c = 8.3816(4)$ Å, $Z = 2$) and is isostructural with the oxide $KCoO_2$. Hafnium is coordinated to five nitrogens in a distorted square base pyramidal geometry, forming layers of edge-sharing pyramids which stack along the *c* axis. Barium is situated between the Hf–N layers and is coordinated to five nitrogen atoms. Samples exhibit temperature-dependent paramagnetism between approximately 8 and 293 K and become superconducting below 8 K.

INTRODUCTION

During the past few years the interest in the chemistry of the ternary and higher order transition metal nitrides has increased significantly (1, 2). This has been due primarily to their unusual crystal and valence chemistry, speculation regarding their physical properties, and potential applications and exciting developments in the preparative routes to these materials (3). Binary and ternary nitride compounds exhibit diverse and often novel crystal structures in which transition metal ions frequently display unusual oxidation states and/or coordination to nitrogen and these are commonly lower than those seen in oxide chemistry (1, 2, 4, 5). For example, trivalent cations, M^{3+}, such as V^{3+}, Cr^{3+}, Mn^{3+}, and Fe^{3+} form ternary nitride structures containing discrete trigonal-planar $[MN_3]^{6-}$ anionic species, isoelectronic with the carbonate ion (4, 5). Late first-row transition metals (Co, Ni, Cu) typically form linear species with nitrogen in which their formal oxidation state is $+1$ (6, 7).

In addition to some unique structures, nitrides also adopt structural types seen in oxide and carbide chemistry. This tendency is perhaps reflective of the intermediate nature of the metal–nitrogen bond. For instance, CaNiN has the YCoC structure (6) whereas Ba_2VN_3 crystallizes in the Rb_2TiO_3 structure (8). The analogies with oxide crystal chemistry are dominant in ternary nitrides of the stoichiometry AMN_2 (A = alkali metal, alkaline earth metal, or transition metal; M = transition metal or lanthanide). The majority of Group 1 transition metal nitrides form layered structures similar to those seen in ternary oxide and chalcogenide chemistry. The $LiMN_2$ (M = Mo, W) materials are hexagonal layered compounds with Mo or W coordinated to six nitrogens in trigonal-prismatic coordination (9, 10) and are Pauli paramagnetic and metallic. The alkali metal nitrides $ATaN_2$ (A = K, Rb, Cs) have structures related to that of β-cristobalite whereas the ternary nitrides $NaMN_2$ (M = Nb, Ta) have the layered α-$NaFeO_2$ structure (11–13).

Mixed transition metal nitrides such as $MnWN_2$, $CoWN_2$, $NiWN_2$ (14, 15), $Fe_{0.8}Mo_{1.2}N_2$ (16), and $FeWN_2$ (17) are structurally similar to $LiMoN_2$ with alternating layers of A–N octahedra and M–N trigonal prisms and are also metallic and paramagnetic. $CuTaN_2$, however, crystallizes in the α-$CuFeO_2$-type (delafossite) structure (18).

Alkaline earth ternary nitrides of formula AMN_2 are less well-known, although recently several new compounds have been reported. $BaCeN_2$ possesses a layered structure and is isostructural with β-$RbScO_2$ (19). $BaZrN_2$ is isotypic with $KCoO_2$, which contains layers made up of edge-sharing Zr–N square-base pyramids (20). The nitrides $SrZrN_2$, $SrHfN_2$ (21), and $CaTaN_2$ (22) all form structures isotypic with α-$NaFeO_2$. The latter tantalum material has attracted particular interest on account of the superconducting transition reported in this nitride at ca. 9.6 K. Magnetic measurements conducted on $SrZrN_2$ and $SrHfN_2$ suggest these materials are intrinsically diamagnetic at room

[1] To whom correspondence should be addressed.

0022-4596/98 $25.00

temperature (21). $BaZrN_2$, however, shows anomalous magnetic behavior for a material of presumed $s = 0$ electronic configuration, exhibiting temperature-independent paramagnetism between 20 and 300 K (20).

We report here the synthesis and structure of the new layered AMN_2 nitride $BaHfN_2$ and the preparation and characterization of the solid solution $BaHf_{1-x}Zr_xN_2$. We also present an investigation of the magnetic properties of these compounds and describe structural relationships to other AMX_2 phases.

EXPERIMENTAL

Starting Materials

The binary nitride Ba_3N_2 was prepared by the reaction of the molten alkaline earth metal–sodium alloy with dried nitrogen at 520°C. The alloy was made by adding clean Ba metal (Alfa, 99 + %) to molten sodium (Aldrich, 99.95%) in a stainless steel crucible at 250°C in an argon-filled glovebox. The cooled crucible of alloy was contained in a stainless steel vessel and heated to 520°C under a positive pressure of nitrogen, monitored by a pressure transducer, until the gas pressure remained constant. Excess sodium was removed by heating under vacuum at 350°C for 24 h. Liquid sodium is unreactive toward nitrogen and serves as an inert solvent for the alkaline earth metals. This method was found to produce nitrides containing negligible amounts of alkaline earth oxide. The reactions yielded crystalline samples of the dark red-black binary nitride. The identity of the nitride was confirmed by powder X-ray diffraction (PXD) with reference to the JCPDS database (card number 27–39).

Synthesis of $BaHfN_2$ and Members of the Solid Solution $BaHf_{1-x}Zr_xN_2$

Polycrystalline samples of $BaHfN_2$ were prepared by the high-temperature solid state reaction of the binary alkaline earth nitride Ba_3N_2 and hafnium nitride (HfN) (Aldrich, 99%) powders. All manipulations were carried out in an evacuable glovebox (ca. 5 ppm O_2, < 5 ppm H_2O) filled with either argon (synthesis preparation) or nitrogen (X-ray diffraction sample preparation). The alkaline earth nitride and HfN powders were thoroughly mixed, ground together in a 1 : 2 molar ratio, and compressed into pellets using a hand press. The resulting pellets were wrapped in molybdenum foil and placed in stainless steel crucibles which were subsequently spot welded closed under argon. The crucibles were fired in a tube furnace at 1000°C for 5 days under flowing argon to prevent oxidation of the steel and then cooled at 20°C/h to room temperature under flowing argon. The cooled crucibles were cleaned and opened in a nitrogen-filled glovebox. From visual examination, there appeared to be no apparent reaction of the nitrides with the Mo foil and the resulting $BaHfN_2$ powder was orange–brown.

Samples of $BaHf_{1-x}Zr_xN_2$ ($x = 0.25, 0.5, 0.75, 1$) were prepared in a manner similar to that used for $BaHfN_2$ by the reaction of Ba_3N_2 and the appropriate amounts of ZrN (Johnson Matthey, 99%) and HfN, maintaining the overall ratio Ba_3N_2 : (Hf, Zr)N 1 : 2. The alkaline earth and Group 4 binary nitrides were thoroughly mixed, pelleted, and wrapped in molybdenum foil as detailed in the preceding paragraph. The Mo tubes were then placed in stainless steel crucibles and spot welded closed under argon. Crucibles were fired at 1000°C for 5 days under flowing argon and then cooled at 20°C/h to room temperature under flowing argon. The cooled crucibles were cleaned and opened in a nitrogen-filled glovebox. As with $BaHfN_2$, there was no apparent reaction of nitrides with the Mo foil and the resulting $BaHf_{1-x}Zr_xN_2$ powders varied in color from orange–brown to deep red as the amount of Zr (x) increased. Both the nitridohafnate, $BaHfN_2$, and the $BaHf_{1-x}Zr_xN_2$ samples were very reactive to air and moisture, reacting to evolve ammonia readily.

Characterization and Structure Determination

Powder X-ray diffraction (PXD) data were collected using a Philips XPERT θ–2θ diffractometer using Cu$K\alpha$ radiation. In a nitrogen-filled glovebox samples were loaded onto an aluminum slide contained in an aluminum holder with a Mylar film window and a threaded, removable cover with an O-ring seal. This arrangement allowed the collection of powder data of air-sensitive materials without interference from Mylar diffraction peaks and is described more fully elsewhere (23). Initially, ca. 60-min scans were taken of each sample over a 2θ range of 5°–80° to assess phase purity and to determine lattice parameters. Phase identification was carried out using the IDENTIFY routine (part of the Philips diffraction software package) on a PC which allows access to the JCPDS database. Samples of $BaHfN_2$ were shown to contain small amounts of BaO, Ba, and HfN. The $BaHf_{1-x}Zr_xN_2$ samples also contained small amounts of ZrN. Ba impurity phases are to be expected in the products from the excess Ba generated from the reactant stoichiometries. Any finely divided Ba metal is easily oxidized by low levels of oxygen. Although HfN and ZrN are not the expected reaction products, not all the Ba_3N_2 may necessarily react with the Group 4 binary nitrides. Furthermore, "Ba_3N_2" is to some extent a nominal stoichiometry; the structure of the alkaline earth binary nitride is not well elucidated (24). The remaining peaks of each pattern were indexed using a combination of the PC software programs VISSER (25), DICVOL91 (26, 27), and TREOR90 (28).

Space groups were derived from systematic absences and cell parameters were refined by least-squares fitting. $BaHfN_2$ and $BaHf_{1-x}Zr_xN_2$ samples were found to be

tetragonal ($P4/nmm$) and deduced to be isostructural with $BaZrN_2$ (itself isostructural with $KCoO_2$) by comparison with a theoretical powder pattern generated by LAZY PULVERIX (29).

Diffraction data suitable for Rietveld refinement were collected at approximately 298 K for $BaHfN_2$ over the 2θ range 5°–130° with a step size of 0.02° 2θ. Scans were run for approximately 17 h. Reaction with air over this time scale, even using the "airtight" containers described, was problematical. The profiles of these samples show significant broadening of peaks associated with $BaHfN_2$ and the appearance of new peaks that could not be identified. Data collected over much shorter times, although showing less evidence of reaction with air, proved to be of too low a quality for accurate refinement, and best results were obtained by doubling the thickness of Mylar film (0.2 mm) in the windows of the aluminum PXD holders and collecting data over longer times. A full-profile Rietveld refinement (30) of $BaHfN_2$ was performed using the Phillips PC RIETVELD PLUS (31, 32) package for 6251 profile points with the $BaZrN_2$ structure (20) as an initial model and with cell parameters obtained from least-squares fitting of PXD data. Peak shapes were modeled using the pseudo-Voigt function and the background was refined as a polynomial function.

Initial cycles in the refinement of $BaHfN_2$ allowed for the variation of the scale factor, zero point, and lattice parameters. As the refinement progressed, atomic positions and peak width parameters were introduced. In the final cycles, isotropic temperature factors were introduced. Although isotropic temperature factors could be refined smoothly for the metal and nitrogen sites, attempts to vary temperature factors of atomic sites anisotropically were unsuccessful. Impurity phases of BaO, Ba, and HfN were simultaneously refined.

The structure of $BaZrN_2$ has been previously determined by X-ray and neutron powder diffraction (20). However, samples of $BaZrN_2$ were selected for structure refinement using PC RIETVELD PLUS for two reasons: first to compare structural data with data previously published for $BaZrN_2$ and with data of $BaHfN_2$ and second to determine quantitatively the amount of impurity phases in our samples. The refinement procedure for $BaZrN_2$ was identical to that for $BaHfN_2$, although varying the isotropic temperature factor for the N1 ($\frac{3}{4}, \frac{1}{4}, \frac{1}{4}$) site led to destabilization of the refinement and thus it was consequently fixed at a value similar to those of the other sites. Impurity phases of BaO, Ba, and ZrN were simultaneously refined.

Quantitative analysis of the diffraction data was performed for each of the ternary nitrides running as part of the PC RIETVELD PLUS package. This yielded weight percentage values of 6.1% BaO, 4.9% Ba, and 1.7% HfN for the $BaHfN_2$ sample and values of 11.7% ZrN, 10.4% Ba, and 7.8% BaO for the $BaZrN_2$ sample.

Magnetic Measurements

Magnetic susceptibility measurements were performed on $BaHfN_2$ and $BaHf_{1-x}Zr_xN_2$ ($x = 0.25, 0.5, 0.75, 1$) samples at room temperature (297 K) using a Johnson Matthey magnetic susceptibility balance. Samples of these compositions (ca. 0.15 g) were thoroughly ground and loaded into preweighed silica sample tubes in an argon-filled glovebox. Sample tubes were filled to a height of ca. 1.5 cm and sealed. The calculated mass susceptibility values were corrected for the measured diamagnetism of the sample tubes.

Variable-temperature magnetic measurements of $BaHfN_2$ and $BaZrN_2$ samples (ca. 0.3 g) were taken using a Cryogenic S100 SQUID susceptometer with a scan length of 3 cm to reduce field inhomogeneity to 0.5%. Data were collected between 5 K and room temperature, cooling first to 5 K at zero field and then subsequently warming under a field of 100 G. Measurements were taken at 2 K steps between approximately 5 and 100 K and at every 4 K between 100 K and room temperature. Additional measurements over regions of specific interest were made with a smaller temperature step as necessary. The magnetic moment at each point was calculated from an average of four scans. All data were corrected for the diamagnetic contribution of the sample holders (either silica or gelatin capsules).

RESULTS AND DISCUSSION

Powder X-ray diffraction data reveal that all compositions $BaHf_{1-x}Zr_xN_2$ ($x = 0, 0.25, 0.5, 0.75, 1$) can be successfully indexed in tetragonal space group $P4/nmm$ (No. 129), adopting the $KCoO_2$ structure as previously proposed for $BaZrN_2$ (20). The powder X-ray patterns of these phases show a small, but discernible, downward shift in 2θ with increasing zirconium content, consistent with the very small size difference between the Hf^{4+} and Zr^{4+} cations. The clearest indication of a true solid solution in the PXD patterns is perhaps the decrease in relative intensity of key peaks such as the 001 as lighter Zr replaces Hf. All compositions contain BaO and Ba as would be expected from the reactant stoichiometries in addition to traces of HfN and ZrN, which decrease and increase, respectively, with increasing Zr content.

The changes in cell parameters with the nominal zirconium content x are shown in Fig. 1. The impact on the unit cell of substituting Zr for Hf is not that profound, as might be anticipated, with only a $\sim$2% increase in cell volume from $BaHfN_2$ ($V \approx 142.8$ Å^3) to $BaZrN_2$ ($V \approx 145.3$ Å^3). The increase in cell volume is brought about almost exclusively by expansion in the ab plane with increased Zr content. This expansion is approximately linear with x. There is little elongation along c from $BaHfN_2$ to $BaZrN_2$ and aside from slight fluctuations in the data, c is almost independent of

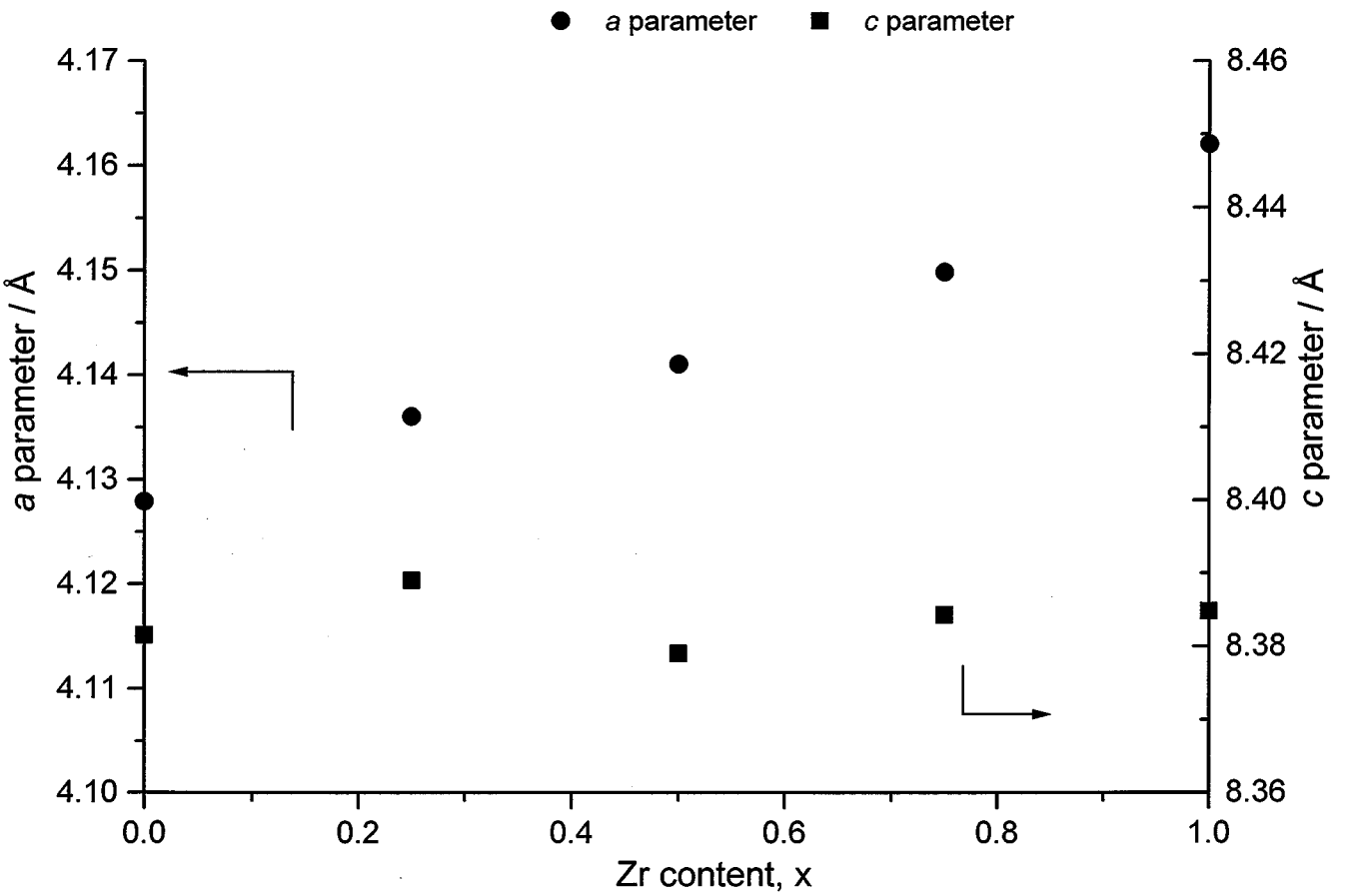

FIG. 1. Plot of a parameter (solid circles) and c parameter (solid squares) against nominal Zr content, x, in $BaHf_{1-x}Zr_xN_2$ samples.

x in $BaHf_{1-x}Zr_xN_2$ samples. Consequently, the c/a ratio decreases from 2.03 in $BaHfN_2$ to 2.01 in $BaZrN_2$.

The final crystallographic results for $BaHfN_2$ are shown in Table 1. The observed, calculated, and difference profiles for the refinement are shown in Fig. 2. Important interatomic distances in $BaHfN_2$ are shown in Table 2. Bond angles around the metal atoms and nitrogen atoms are described in Tables 3 and 4, respectively. $BaHfN_2$ (Fig. 3) is isotypic with $KCoO_2$ and $BaZrN_2$ (20). The structure is made up of $[HfN_2]^{2-}$ anions and Ba^{2+} cations. The nitridohafnate anions are composed of Hf atoms surrounded by nitrogens in fivefold, square-base pyramidal coordination. Each square-base pyramid has a bent basal plane and overall C_{4v} point symmetry. The $[HfN_2]^{2-}$ anions are linked by the edges of the pyramid bases to form layers in which the apices of adjoining pyramids are aligned alternatively up and down parallel to the c axis (Fig. 4). The Ba^{2+} cations are situated between these Hf–N sheets level with the pyramid apices.

The square-base pyramidal nitridohafnate anions are compressed along the c axis, resulting is one shorter apical Hf–N2 bond at 2.05(2) Å and four longer basal Hf–N1 bonds at 2.1856(5) Å. The basal nitrogens are bent away from the plane of the hafnium to produce an N1–Hf–N1 angle of significantly less than 180° (~141.6°). The central Hf

TABLE 1
Final Crystallographic Results for $BaHfN_2$

Space group $P4/nmm$, $a = 4.1279(1)$ Å, $c = 8.3816(4)$ Å
$R_I = 2.58\%$, $R_p = 7.80\%$, $R_{wp} = 10.43\%$, $R_e = 0.96\%$

Atom	Site	x	y	z	B^a (Å^2)	N^b
Ba	2c	0.25	0.25	0.8479(2)	0.82(5)	1.0
Hf	2c	0.25	0.25	0.4142(1)	1.03(5)	1.0
N1	2b	0.75	0.25	0.5	1.4(6)	1.0
N2	2c	0.25	0.25	0.168(2)	4.3(8)	1.0

[a] $B = \frac{4}{3}[a^2B_{11} + b^2B_{22} + c^2B_{33} + ab(\cos\gamma)B_{12} + ac(\cos\beta)B_{13} + bc(\cos\alpha)B_{23}]$.
[b] N defines the fractional site occupancy.

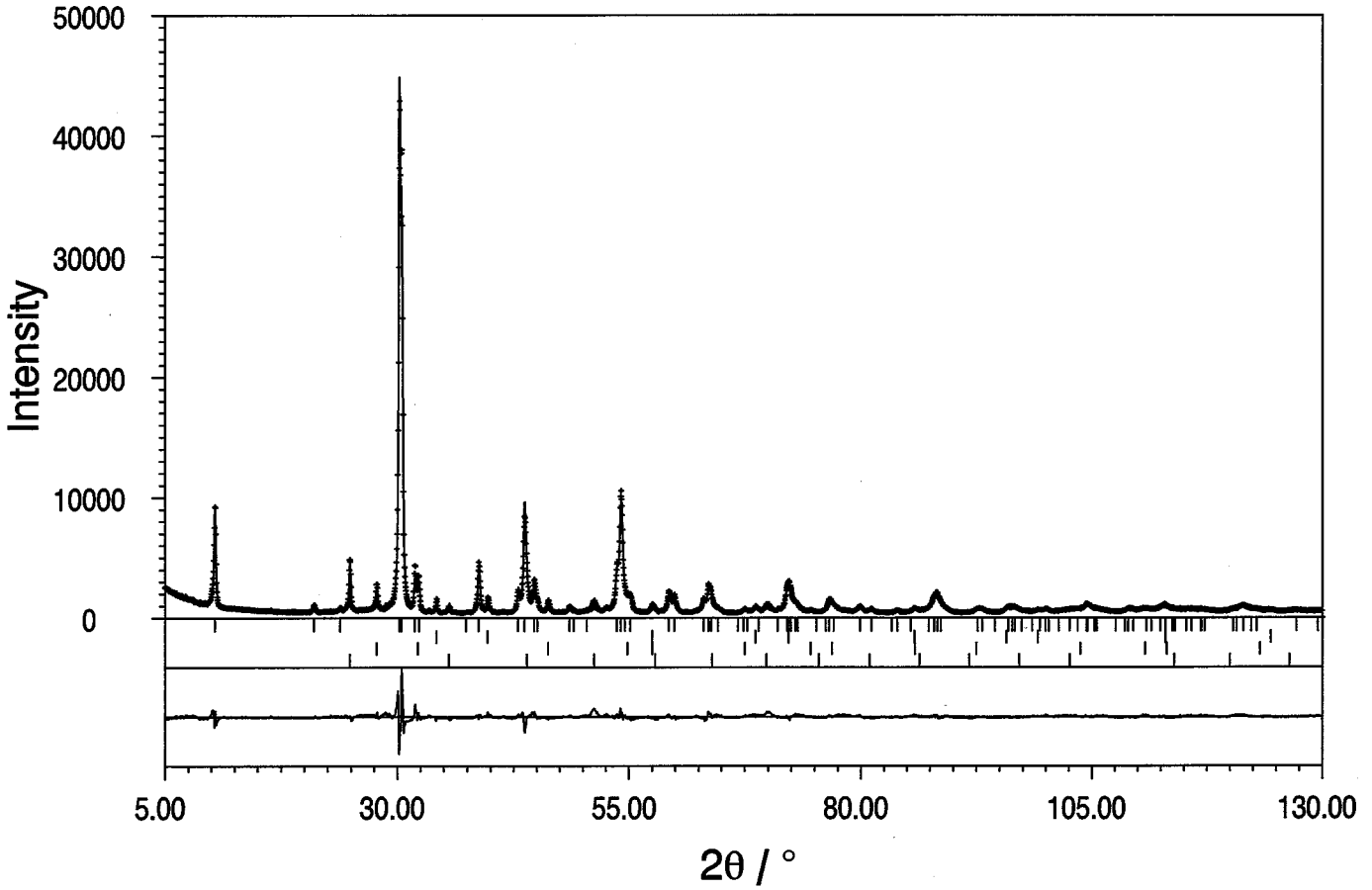

FIG. 2. Observed, calculated, and difference profiles for $BaHfN_2$.

atom consequently sits ≈ 0.72 Å above the plane of the basal nitrogens. This configuration of the $[HfN_2]^{2-}$ anion is almost identical to that previously observed in the nitridozirconate anion in $BaZrN_2$, where the apical distances of the pyramids were also shorter than the basal metal–nitrogen bonds (20). As in the nitridozirconate, whereas the basal bonds are typical of a metal–nitrogen bond on the basis of ionic radii, the much reduced length of the apical metal–nitrogen distance suggests a multiple Hf–N bond. In fact, the apical M^{IV}–N bond length is unchanged in moving from $BaHfN_2$ to $BaZrN_2$, whereas the basal distances lengthen, stressing the different nature of the two (apical

TABLE 2
Interatomic Distances in $BaHfN_2$

Atoms	Number	Distance (Å)
Ba–N1	4	3.572(1)
Ba–N2	1	2.68(2)
Ba–N2	4	2.922(1)
Hf–N1	4	2.1856(5)
Hf–N2	1	2.05(2)
Ba–Hf	1	3.635(2)
Ba–Hf	4	3.653(1)
Hf–Hf	4	3.254(1)

TABLE 3
Bond Angles around Ba and Hf in $BaHfN_2$

Atoms	Angle (deg)	Atoms	Angle (deg)
N1–Ba–N1	70.582(4) × 2	N1–Hf–N1	83.785(3) × 4
N1–Ba–N1	48.223(3) × 4	N1–Hf–N1	141.580(9) × 2
N1–Ba–N2	111.6(3) × 8	N1–Hf–N2	109.210(5) × 4
N1–Ba–N2	63.4(3) × 8		
N1–Ba–N2	144.709(2) × 4		
N2–Ba–N2	174.5(6) × 2		
N2–Ba–N2	89.86(3) × 4		
N2–Ba–N2	92.7(4) × 4		

TABLE 4
Bond Angles around N1 and N2 in $BaHfN_2$

Atoms	Angle (deg)	Atoms	Angle (deg)
Ba–N1–Ba	131.77(1) × 4	Ba–N2–Ba	87.26(6) × 4
Ba–N1–Ba	70.58(2) × 2	Ba–N2–Ba	89.869(6) × 4
Ba–N1–Hf	74.42(3) × 8	Ba–N2–Ba	174.5(1) × 2
Ba–N1–Hf	73.91(4) × 4	Ba–N2–Hf	92.73(6) × 4
Ba–N1–Hf	144.50(4) × 4	Ba–N2–Hf	180.0(1)
Hf–N1–Hf	96.21(1) × 4		
Hf–N1–Hf	141.58(5) × 2		

and basal) metal–nitrogen bonds. It is interesting to note that in $KCoO_2$—the oxide analogue of these Group 4 nitrides—there is no significant distortion of the $[CoO_2]^-$ pyramids. In $KCoO_2$, the apical Co–O bond (1.99 Å) and the basal Co–O bonds (1.91 Å) are nearly identical (33).

Known examples of ternary nitridohafnates are not numerous and only one ternary alkaline earth hafnium nitride, $SrHfN_2$, has been previously reported (21). The hafnium coordination in this compound is octahedral, with six distances to nitrogen of 2.273(2) Å. These distances closely approximate the mean Hf–N bond lengths seen in the binary nitrides Hf_3N_2 (2.258 Å) and Hf_4N_3 (2.263 Å) (34) and are typical of an Hf–N bond constructed from a basis of ionic radii (35). That the Hf–N distances are shorter in $BaHfN_2$ (and most notably the apical Hf–N2 bond distance) lends further weight to evidence for the covalent character of the M–N bonding in the barium nitridohafnate. This bonding behavior is mirrored in the nitridozirconates.

The coordination of barium to nitrogen could be regarded as ninefold as in $BaZrN_2$ (20) but is effectively only fivefold (square pyramidal), with the longer "basal" distances (Ba–N1) of the Ba–N polyhedron being over 3.5 Å (3.572(1) Å). The mean Ba–N bond length, including the four longer distances, is 3.184(3) Å, whereas, excluding these distances, it is more reasonably 2.874(4) Å. This distance is of the same order as those seen in other barium ternary nitrides (e.g., 2.88(1) Å in $BaCeN_2$ (19) and a mean distance of 2.914(5) Å in Ba_3CrN_3 (23)). The distances agree well with the mean values calculated from those bond lengths previously reported for $BaZrN_2$ (3.212(3) and 2.913(3) Å including and excluding the longer Ba–N distances, respectively) (20). The overall effect of replacing Zr by smaller Hf is to reduce slightly the size of the Ba–N polyhedron. The major contribution to the increase in cell volume (and a) with x in the $BaHf_{1-x}Zr_xN_2$ solid solution can therefore be attributed to the lengthening of the basal M–N distances as Zr replaces Hf.

The nitrogen atoms are coordinated to four and six metal atoms, respectively. N1 is coordinated in a distorted tetrahedral geometry to four hafnium atoms whereas N2 is coordinated in a distorted octahedral geometry to five barium atoms and one hafnium atom. The N2–M octahedron is compressed along z. The compression of the anion- and cation-centered polyhedra along z is reflected in the c/a ratio of $BaHfZ_2$ (2.03) and $BaZrN_2$ (2.01) compared to $KCoO_2$ (2.08), where the coordination environments are less distorted (33).

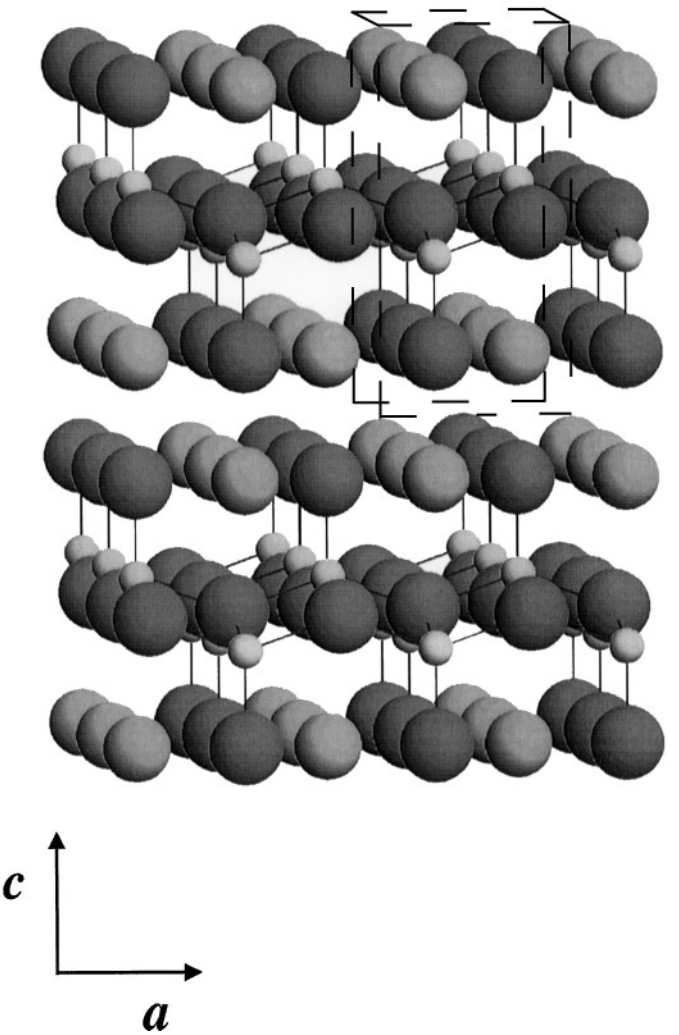

FIG. 3. Structure of $BaHfN_2$ showing layers of $[HfN_2]^{2-}$ anions and Ba^{2+} cations stacked along the c axis. Ba atoms are denoted by medium light spheres, Hf atoms by small light spheres, and N atoms by large dark spheres. The unit cell is delineated by the dashed line.

Bond valence calculations were performed for $BaHfN_2$ and $BaZrN_2$ using the bond length parameters proposed by Brese and O'Keeffe for compounds with anions other than oxygen, fluorine, or chlorine (36, 37). The bond valence parameters used for Ba–N, Hf–N, and Zr–N were 2.47, 2.09, and 2.11 Å, respectively. The calculated site valences for $BaHfN_2$ and $BaZrN_2$ are shown in Table 5 together with those calculated from crystallographic data from other

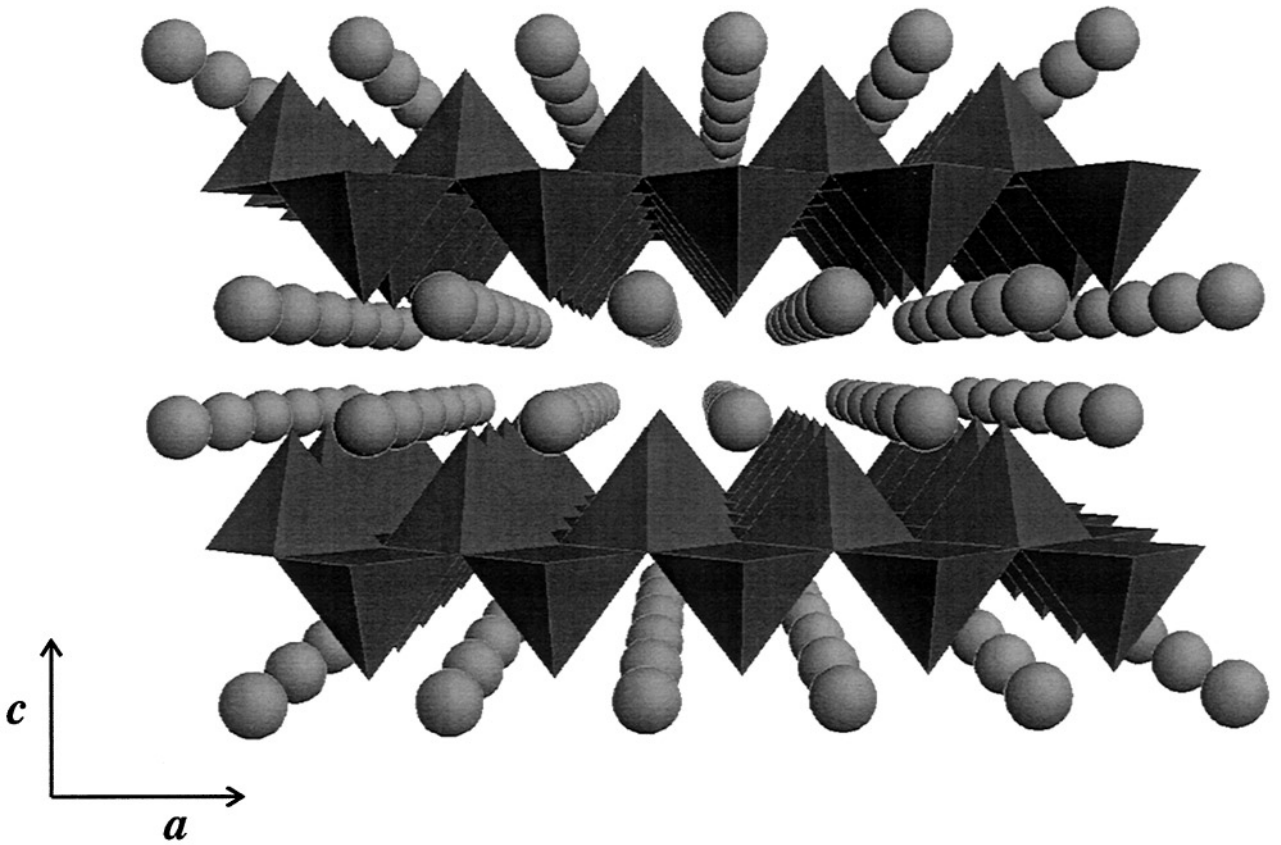

FIG. 4. Perspective view of the extended structure of $BaHfN_2$ showing layers of edge-sharing $[HfN_2]^{2-}$ square-based pyramidal anions, with apices alternately up and down, parallel to the 001 plane.

alkaline earth metal AMN_2 phases. Although the site valence for N2 in both compounds is a little low, the most noticeable result of the bond valence calculations is the very low value for the Ba site. The Ba site valence increases to 1.95(4) in $BaHfN_2$ and 1.87(4) in $BaZrN_2$ if the four Ba–N1 interactions at $\sim$3.5 Å are taken into account. However, this also has the effect of increasing the N1 site valences to 3.29(1) and 3.28(1) in $BaHfN_2$ and $BaZrN_2$, respectively. Alkaline earth site valences (especially Ba and Sr) are frequently observed to be lower than expected in binary and ternary nitrides. This suggests that either the *A*–N bonds are longer than expected or the formal oxidation state is lower than one would naturally anticipate. This latter possibility seems appropriate particularly for alkaline earth metal binary phases A_2N, where the stoichiometry implies an oxidation state of 1.5 for the metal cation and perhaps a degree of metallic bonding. In fact, the Ba–Ba distances (3.875(1) Å in $BaHfN_2$ and 3.902(1) Å in $BaZrN_2$), *M*–*M* distances, and Ba–*M* distances in these nitrides are all within, or close to, the distances approximated from addition of metallic radii values (38).

TABLE 5
Calculated Site Valencies in $A^{II}M^{IV}N_2$ Materials

Nitride	*A*-site valence	*M*-site valence	N1-site valence	N2-site valence	Derived from ref
$BaHfN_2$	1.75(4)	4.20(6)	3.09(1)	2.86(9)	This work
$BaZrN_2$	1.74(1)	4.4(1)	3.34(2)	2.8(1)	20
$BaZrN_2$	1.67(2)	4.25(4)	3.074(4)	2.85(5)	This work
$SrHfN_2$	2.15(2)	3.68(2)	2.92(2)		21
$SrZrN_2$	2.19(2)	3.65(2)	2.93(2)		21
$BaCeN_2$	1.98(6)	4.7(1)	3.38(7)		19

The Hf and Zr site valences are higher than expected from the nominal stoichiometries and this appears characteristic of transition metal sites in ternary nitrides (1, 23). This can usually be attributed to one or more multiple *M*–*N* bonds giving rise to distances that are shorter than expected on a purely ionic basis. The bond valence calculations emphasize the multiple character of the *M*–N2 bond in particular.

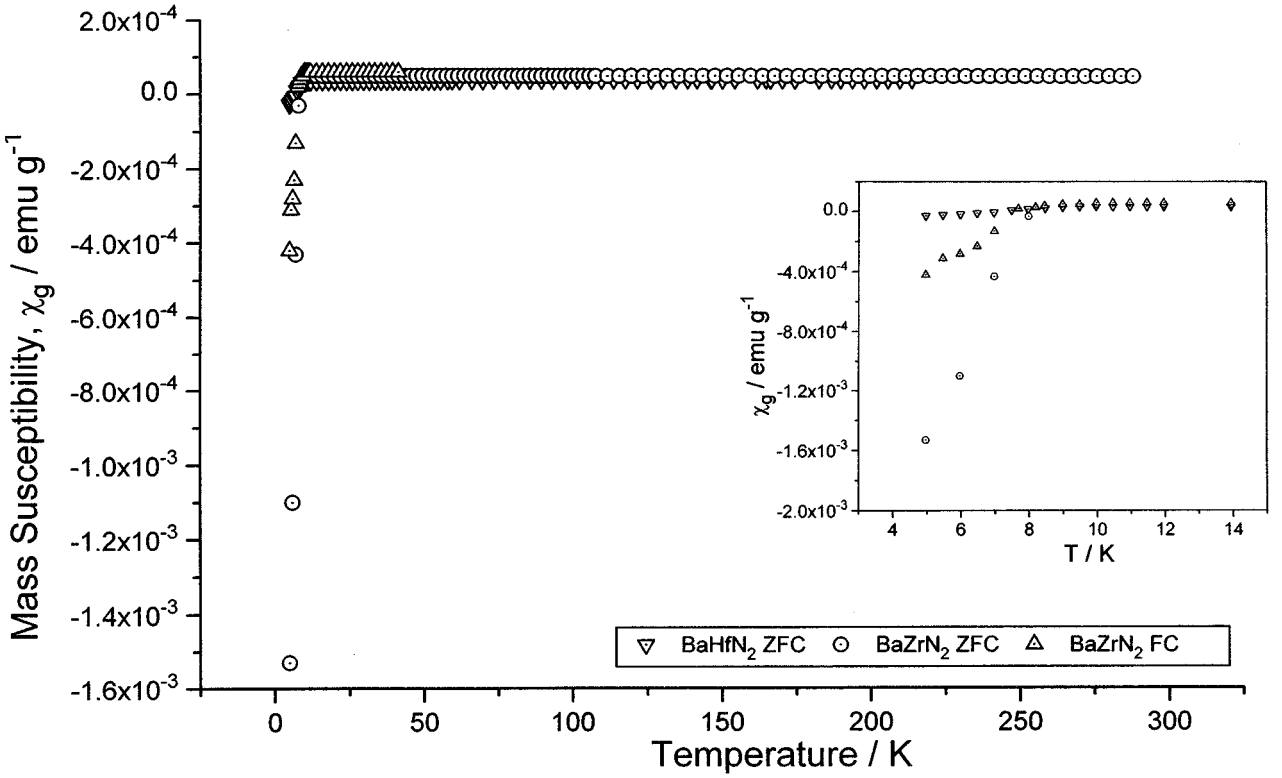

FIG. 5. Variation of the measured mass susceptibility with temperature for $BaHfN_2$ and $BaZrN_2$ showing detail of behavior close to T_c (inset).

Indeed, were this bond length of the same order as the M–N1 distances, the site valences for Hf and Zr would be ~3.9 and ~3.8. The site valences obtained perhaps highlight the deficiencies in using the bond valence model for these compounds, in which covalent and metallic, as well as ionic, contributions are clearly significant in the overall bonding scheme.

Values for the total mass susceptibility, χ_g, of 2.895×10^{-5} and 3.753×10^{-5} emu g^{-1} were obtained for the $x = 0$ nitridohafnate and the $x = 1$ nitridozirconate, respectively, at room temperature (293 K). The intermediate members of the solid solution $BaHf_{1-x}Zr_xN_2$ with $x = 0.25$, 0.5, and 0.75 gave values for χ_g of 3.183×10^{-5}, 3.078×10^{-5}, and 3.634×10^{-5} emu g^{-1}, respectively, at the same temperature. These values might suggest that the materials may not be diamagnetic, as would be expected for pure Hf(IV) and Zr(IV) ($S = 0$) compounds. However, PXD has revealed the ternary nitride preparations to contain varying amounts of HfN and ZrN across the solid solution and these phases are perhaps the more likely origin of the paramagnetic contribution at room temperature. Until our synthetic routes to the new nitrides progress yet further to effectively reduce impurity levels to minimal values, a detailed discussion of the susceptibility values is not appropriate.

The results of variable-temperature magnetic measurements for $BaHfN_2$ and $BaZrN_2$ are shown in Fig. 5. These confirm the room temperature findings and show that samples are paramagnetic between approximately 300 and 8 K. As previously observed for $BaZrN_2$ between 20 and 300 K (20), this paramagnetic behavior is essentially temperature independent. Below the approximate lower temperature limit the samples become superconducting. The T_c onset temperatures are at ~8.9 and ~9.5 K for $BaHfN_2$ and $BaZrN_2$, respectively. The binary Group 4 nitrides HfN and ZrN are paramagnetic at room temperature and become superconducting at low temperature with T_cs of 8.83 and 10.0 K, respectively (39), and it seems likely that the superconductivity observed in the ternary nitride samples arises from the above binary nitride impurities (HfN, ZrN) rather than from the intrinsic behavior of the ternary nitrides themselves (as, for example, in $CaTaN_2$ (22)). However, at present, we have not succeeded in making phase-pure samples of $BaHfN_2$ or $BaZrN_2$ and therefore cannot conclusively state that the ternary nitrides are nonsuperconducting.

In summary, we have synthesized the series of new ternary nitrides $BaHf_{1-x}Zr_xN_2$ and elucidated the structure of $BaHfN_2$ from powder X-ray diffraction data. The bonding in these new materials shows not only ionic but also

covalent and metallic character. The developing synthetic strategies to ternary nitrides, some illustrated here, point to yet further developments in this rich, but still relatively unexplored, area of solid state chemistry.

ACKNOWLEDGMENTS

We thank the EPSRC for supporting this work, for the postdoctoral fellowship for D.H.G., and recently for the award of an Advanced Fellowship to D.H.G. We also thank The Royal Society for the award of a Leverhulme Senior Reserach Fellowship to P.P.E.

REFERENCES

1. N. E. Brese and M. O'Keeffe, *Struct. Bonding* (*Berlin*) **79,** 307 (1992).
2. F. J. DiSalvo and S. J. Clarke, *Curr. Opin. Solid State Mater. Sci.* **1,** 241 (1996).
3. For example, see F. J. DiSalvo, *Science* **247,** 649 (1990).
4. For example, see D. A. Vennos, M. E. Badding, and F. J. DiSalvo, *Inorg. Chem.* **29,** 4059 (1990).
5. For example, see P. Höhn, R. Kniep, and A. Rabenau, *Z. Kristallogr.* **153,** 153 (1991).
6. M. Y. Chern and F. J. DiSalvo, *J. Solid State Chem.* **88,** 459 (1990).
7. For example, see A. Tennstedt and R. Kniep, *Z. Anorg. Allg. Chem.* **620,** 1781 (1994).
8. D. H. Gregory, M. G. Barker, P. P. Edwards, and D. J. Siddons, *Inorg. Chem.* **34,** 3912 (1995).
9. S. H. Elder, L. H. Doerrer, F. J. DiSalvo, J. B. Parise, D. Guyomard, and J. M. Tarascon, *Chem. Mater.* **4,** 928 (1992).
10. P. S. Herle, M. S. Hegde, N. Y. Vasanthacharya, J. Gopalakrishnan, and G. N. Subbanna, *J. Solid State Chem.* **112,** 208 (1994).
11. H. Jacobs and E. von Pinkowski, *J. Less-Common Met.* **146,** 147 (1989).
12. P. E. Rauch and F. J. DiSalvo, *J. Solid State Chem.* **100,** 160 (1992).
13. H. Jacobs and B. Hellmann, *J. Alloys Compd.* **191,** 51 (1993).
14. J. Grins, P.-O. Käll, and G. Svensson, *J. Mater. Chem.* **5**(4), 571 (1995).
15. P. S. Herle, N. Y. Vasanthacharya, M. S. Hedge, and J. Gopalakrishnan, *J. Alloys Compd.* **217,** 22 (1995).
16. D. S. Bem, H. P. Olsen, and H.-C. zur Loye, *Chem. Mater.* **7,** 1824 (1995).
17. D. S. Bem and H.-C. zur Loye, *J. Solid State Chem.* **104,** 467 (1993).
18. U. Zachwieja and H. Jacobs, *Eur. J. Solid State Inorg. Chem.* **28,** 1055 (1991).
19. O. Seeger and J. Strähle, *Z. Naturforsch., B* **49,** 1169 (1994).
20. O. Seeger, M. Hoffmann, J. Strähle, J. P. Laval, and B. Frit, *Z. Anorg. Allg. Chem.* **620,** 2008 (1994).
21. D. H. Gregory, M. G. Barker, P. P. Edwards, and D. J. Siddons, *Inorg. Chem.* **35,** 7608 (1996).
22. V. Balbarin, R. B. Van Dover, and F. J. DiSalvo, *J. Phys. Chem. Solids* **57,** 1919 (1996).
23. M. G. Barker, M. J. Begley, P. P. Edwards, D. H. Gregory, and S. E. Smith, *J. Chem. Soc., Dalton Trans.* 1 (1996).
24. For example, see S. M. Ariya, E. A. Prokofyeva, and I. I. Matveeva, *J. Gen. Chem. USSR* **25,** 609 (1955).
25. J. W. Visser, *J. Appl. Crystallogr.* **2,** 89 (1969).
26. D. Louer and M. Louer, *J. Appl. Crystallogr.* **5,** 271 (1972).
27. A. Boultif and D. Louer, *J. Appl. Crystallogr.* **24,** 987 (1991).
28. P.-E. Werner, L. Eriksson, and M. Westdahl, *J. Appl. Crystallogr.* **18,** 367 (1985).
29. K. Yvon, W. Jeitschko, and E. Parthe, *J. Appl. Crystallogr.* **10,** 73 (1977).
30. H. M. Rietveld, *J. Appl. Crystallogr.* **2,** 65 (1969).
31. D. B. Wiles and R. A. Young, *J. Appl. Crystallogr.* **14,** 149 (1981).
32. C. J. Howard and R. J. Hill, AAEC Report No. M112, 1986.
33. M. Jansen and R. Hoppe, *Z. Anorg. Allg. Chem.* **417,** 31 (1975).
34. E. Rudy, *Metall. Trans.* **1,** 1249 (1970).
35. R. D. Shannon and C. T. Prewitt, *Acta Crystallogr., B* **25,** 925 (1969).
36. N. E. Brese and M. O'Keeffe, *J. Am. Chem. Soc.* **113,** 3226 (1991).
37. N. E. Brese and M. O'Keeffe, *Acta Crystallogr., B* **47,** 192 (1991).
38. A. F. Wells, "Structural Inorganic Chemistry," 5th ed. Clarendon Press, Oxford, 1984.
39. L. E. Toth, "Transition Metal Carbides and Nitrides." Academic Press, New York, 1971.